



HAL
open science

Bianchi I meets the Hubble diagram

Thomas Schucker, André Tilquin, Galliano Valent

► **To cite this version:**

Thomas Schucker, André Tilquin, Galliano Valent. Bianchi I meets the Hubble diagram. Monthly Notices of the Royal Astronomical Society, 2014, 444 (3), pp.2820-2836. 10.1093/mnras/stu1656 . hal-00996879

HAL Id: hal-00996879

<https://hal.science/hal-00996879v1>

Submitted on 11 Feb 2025

HAL is a multi-disciplinary open access archive for the deposit and dissemination of scientific research documents, whether they are published or not. The documents may come from teaching and research institutions in France or abroad, or from public or private research centers.

L'archive ouverte pluridisciplinaire **HAL**, est destinée au dépôt et à la diffusion de documents scientifiques de niveau recherche, publiés ou non, émanant des établissements d'enseignement et de recherche français ou étrangers, des laboratoires publics ou privés.

Bianchi I meets the Hubble diagram

Thomas Schücker¹, André Tilquin², Galliano Valent³

Abstract

We improve existing fits of the Bianchi I metric to the Hubble diagram of supernovae and find an intriguing yet non-significant signal for anisotropy that should be verified or falsified in the near future by the Large Synoptic Survey Telescope.

Since the literature contains two different formulas for the apparent luminosity as a function of time of flight in Bianchi I metrics, we present an independent derivation confirming the result by Saunders (1969). The present fit differs from earlier ones by Koivisto & Mota and by Campanelli et al. in that we use Saunders' formula, a larger sample of supernovae, Union 2 and JLA, and we use the general Bianchi I metric with three distinct eigenvalues.

PACS: 98.80.Es, 98.80.Cq

Key-Words: cosmological parameters – supernovae

¹ CPT, Aix-Marseille University, Université de Toulon, CNRS UMR 7332, 13288 Marseille, France
thomas.schucker@gmail.com

² CPPM, Aix-Marseille University, CNRS/IN2P3, 13288 Marseille, France
tilquin@cppm.in2p3.fr

³ CPT, Aix-Marseille University, Université de Toulon, CNRS UMR 7332, 13288 Marseille, France
Sorbonne Universits, UPMC Univ Paris 06, LPTHE CNRS UMR 7589, 75005 Paris, France

1 Introduction

We would like to explain our motivation for the present analysis by comparing cosmology with the description of the earth's surface. In good approximation, this surface is maximally symmetric, i.e. a sphere. We observe a breaking of this symmetry of the order of one per mill by the geography, for example by Mount Everest, $8.8 \text{ km} \cdot 2\pi / (40\,000 \text{ km}) \approx 1.4 \cdot 10^{-3}$. Of course we would not try to describe these geographic deviations in terms of a simple geometric model. But there is a second breaking of the maximal symmetry, of the order of 3 per mill, that we call geometric. Indeed this breaking admits a simple geometric description, in terms of an oblate ellipsoid. Our polar radius is about 21.3 km shorter than the equatorial ones, $21.3 \text{ km} \cdot 2\pi / (40\,000 \text{ km}) \approx 3.3 \cdot 10^{-3}$.

The Robertson-Walker metric of the cosmological standard model has maximal spatial symmetry. The Bianchi I metric, that we consider in the following for its calculational simplicity, is obtained from the flat Robertson-Walker metric by giving up the three isotropies. It is true that we observe anisotropies of the order of 10^{-5} in the cosmic micro-wave background. But we take these to be geographic deviations and do not try to model them by a simple geometry. Our motivation for using the Bianchi I metric is that it might describe a new breaking of maximal symmetry, of geometric type.

Attempts at deciphering an anisotropy in the Hubble diagram are not new. They come in at least three classes.

The first splits the Hubble diagram in two hemispheres, fits both independently and tries to find a splitting direction in which the two fits differ significantly (Kolatt & Lahav 2001; Schwarz & Weinhorst 2007; Antoniou & Perivolaropoulos 2010; Kalus et al. 2013; Yang, Wang & Chu 2013; Jimenez, Salzano & Lazkoz 2014). However there is no solution of Einstein's equations compatible with the split.

A second class is similar, but does the fitting with a modified theory of gravity, e.g. based on Finsler geometry, Chang et al. (2014a,b).

The third class is the most conservative. Start with a (pseudo-) Riemannian geometry admitting less symmetries than the Robertson-Walker metric, mostly Bianchi I, compute redshift and apparent luminosity, solve Einstein's equation and then confront this model with the Hubble diagram of supernovae.

We are aware of two analyses of this type, by Koivisto & Mota (2008a) and by Campanelli et al. (2010). Neither finds a preferred direction in the Hubble diagram.

These analyses rest on four main ingredients: two kinematic formulae, the redshift and the apparent luminosity as functions of the three scale factors, and two dynamical formulae, the Einstein equation and its solutions with cosmological constant and dust. Both analyses (Koivisto & Mota 2007a; Campanelli et al. 2010) take the first three ingredients from Koivisto & Mota (2008b) and presumably solve the Einstein equation numerically with a Runge-Kutta algorithm.

All mentioned authors seem to be unaware of a work by Saunders (1969) giving all four ingredients. His apparent luminosity and his Einstein equation disagree with the formulae by Koivisto & Mota (2008b). The disagreement on the apparent luminosity is particularly bothersome: Saunders derives it using a result from an earlier paper by himself which in turn relies on a theorem by Ehlers and Sachs. Koivisto & Mota (2008b) on the other hand derive

the apparent luminosity in eight lines.

In the present paper we give *ab initio* derivations of the four ingredients. Our luminosity agrees with Saunders' and our Einstein equation agrees with Koivisto & Mota's. Therefore we redo the fit to the supernovae. We also include recent data and extend the fit to the general Bianchi I metric with three distinct eigenvalues.

2 Geodesics

The Bianchi I metric reads

$$d\tau^2 = dt^2 - a(t)^2 dx^2 - b(t)^2 dy^2 - c(t)^2 dz^2, \quad a(t), b(t), c(t) > 0. \quad (1)$$

It is homogeneous but not isotropic. Its non-vanishing Christoffel symbols are:

$$\begin{aligned} \Gamma^t_{xx} &= aa', & \Gamma^t_{yy} &= bb', & \Gamma^t_{zz} &= cc', \\ \Gamma^x_{tx} &= a'/a, & \Gamma^y_{ty} &= b'/b, & \Gamma^z_{tz} &= c'/c, \end{aligned} \quad (2)$$

where we use $' := d/dt$. Thanks to the isometries under translations, the geodesic equations can be integrated once to read,

$$\dot{x} = A/a^2, \quad \dot{y} = B/b^2, \quad \dot{z} = C/c^2, \quad \dot{t}^2 = K + A^2/a^2 + B^2/b^2 + C^2/c^2, \quad (3)$$

where we use $\dot{\cdot} := d/dp$ with an affine parameter p . A , B , C and K are integration constants. We have the time-like solutions $t = p = \tau$, $x = x_0$, $y = y_0$, $z = z_0$ for comoving galaxies, $A = B = C = 0$, $K = 1$. To describe photons going between them we need light-like geodesics, $K = 0$. Let us take the initial conditions at $p = p_{-1}$:

$$\begin{aligned} t &= t_{-1}, & x &= x_{-1}, & y &= y_{-1}, & z &= z_{-1}, \\ \dot{t} &= 1/W_{-1}, & \dot{x} &= A/a_{-1}^2, & \dot{y} &= B/b_{-1}^2, & \dot{z} &= C/c_{-1}^2, \end{aligned} \quad (4)$$

with the abbreviations $a_{-1} := a(t_{-1})$, ... and

$$W(t) := \left(\frac{A^2}{a(t)^2} + \frac{B^2}{b(t)^2} + \frac{C^2}{c(t)^2} \right)^{-1/2}, \quad (5)$$

To simplify notations we put $\vec{x}_{-1} = 0$. Let us say that the photon arrives today $t = t_0$ at comoving position \vec{x}_0 . Then we have:

$$x_0 = \int_{t_{-1}}^{t_0} \frac{A}{a^2} W dt, \quad y_0 = \int_{t_{-1}}^{t_0} \frac{B}{b^2} W dt, \quad z_0 = \int_{t_{-1}}^{t_0} \frac{C}{c^2} W dt. \quad (6)$$

In our conventions the speed of light is unity; proper time τ , the coordinate time t and the affine parameter p have units of seconds, the comoving coordinates x , y , z are dimensionless and the scale factors a , b , c and the integration constants A , B , C carry seconds. Then W is

dimensionless. Through a rescaling of the affine parameter p we may achieve $A^2 + B^2 + C^2 = 1 \text{ s}^2$. Through a rescaling of the coordinates x, y, z we may achieve $a_0 = b_0 = c_0 = 1 \text{ s}$.

We also learnt from equation (3) that in the Bianchi I metric, the position in the sky of luminous sources changes with time (unless they lie in a principle direction, e.g. $B = C = 0$). Since no such drift or ‘cosmic parallax’ (Quercellini, Quartin & Amendola 2009) has been observed today, any deviation of Bianchi type I from maximal symmetry must be small (Fontanini, West & Trodden 2009; Campanelli et al. 2011).

3 Redshift

To compute the redshift of the galaxy at $\vec{x}_{-1} = 0$, let it send out a second go-between an atomic period T later, $t = t_{-1} + T$. The atomic period is very small with respect to the time of flight: $T \ll t_0 - t_{-1}$. We want the second go-between to arrive at the same comoving location \vec{x}_0 where our detector sits. This means that we must slightly change the initial direction of the light-like geodesics coded in the integration constants. Let us call them $\tilde{A}, \tilde{B}, \tilde{C}$. They are close to the former integrations constants:

$$\tilde{A} = A(1 + \alpha), \quad \tilde{B} = B(1 + \beta), \quad \tilde{C} = C(1 + \gamma), \quad \alpha, \beta, \gamma \approx T/(t_0 - t_{-1}). \quad (7)$$

We call the arrival time of the second go-between $t_0 + T_D$. In order to compute the Doppler-shifted atomic period T_D at \vec{x}_0 we have to solve the geodesic equation (3) for the second go-between with integration constants $\tilde{K} = 0, \tilde{A}, \tilde{B}, \tilde{C}$ and initial conditions

$$\dot{t}(p_{-1}) = \sqrt{\frac{\tilde{A}^2}{a_{-1}^2} + \frac{\tilde{B}^2}{b_{-1}^2} + \frac{\tilde{C}^2}{c_{-1}^2}}, \quad \dot{x} = \frac{\tilde{A}}{a_{-1}}, \quad \dot{y} = \frac{\tilde{B}}{b_{-1}}, \quad \dot{z} = \frac{\tilde{C}}{c_{-1}}, \quad (8)$$

with $a_{-1} := a(t_{-1} + T), \dots$ As before the unique solution is:

$$x_0 = \int_{t_{-1}+T}^{t_0+T_D} \frac{\tilde{A}}{a^2} \tilde{W} dt, \quad y_0 = \int_{t_{-1}+T}^{t_0+T_D} \frac{\tilde{B}}{b^2} \tilde{W} dt, \quad z_0 = \int_{t_{-1}+T}^{t_0+T_D} \frac{\tilde{C}}{c^2} \tilde{W} dt, \quad (9)$$

with

$$\tilde{W}(t) := \left(\frac{\tilde{A}^2}{a(t)^2} + \frac{\tilde{B}^2}{b(t)^2} + \frac{\tilde{C}^2}{c(t)^2} \right)^{-1/2}, \quad (10)$$

To first order in $T/(t_0 - t_{-1})$ we get:

$$\begin{aligned} x_0 \approx & \int_{t_{-1}}^{t_0} \frac{A}{a^2} W dt + \alpha \int_{t_{-1}}^{t_0} \frac{A}{a^2} \left(\frac{B^2}{b^2} + \frac{C^2}{c^2} \right) W^3 dt - \beta \int_{t_{-1}}^{t_0} \frac{A}{a^2} \frac{B^2}{b^2} W^3 dt \\ & - \gamma \int_{t_{-1}}^{t_0} \frac{A}{a^2} \frac{C^2}{c^2} W^3 dt - \frac{A}{a_{-1}^2} W_{-1} T + \frac{A}{a_0^2} W_0 T_D. \end{aligned} \quad (11)$$

Together with the first of equations (6) we have:

$$\begin{aligned}
0 &\approx \alpha \int_{t_{-1}}^{t_0} \frac{W^3}{a^2} \left(\frac{B^2}{b^2} + \frac{C^2}{c^2} \right) dt - \beta \int_{t_{-1}}^{t_0} \frac{W^3}{a^2} \frac{B^2}{b^2} dt \\
&\quad - \gamma \int_{t_{-1}}^{t_0} \frac{W^3}{a^2} \frac{C^2}{c^2} dt - \frac{W_{-1}}{a_{-1}^2} T + \frac{W_0}{a_0^2} T_D \\
&= B^2 Z + C^2 Y - \frac{W_{-1}}{a_{-1}^2} T + \frac{W_0}{a_0^2} T_D,
\end{aligned} \tag{12}$$

with

$$X := (\beta - \gamma) \int_{t_{-1}}^{t_0} \frac{W^3}{b^2 c^2} dt, \quad Y := (\alpha - \gamma) \int_{t_{-1}}^{t_0} \frac{W^3}{c^2 a^2} dt, \quad Z := (\alpha - \beta) \int_{t_{-1}}^{t_0} \frac{W^3}{a^2 b^2} dt. \tag{13}$$

Similarly for y_0 ,

$$0 \approx -A^2 Z + C^2 X - \frac{W_{-1}}{b_{-1}^2} T + \frac{W_0}{b_0^2} T_D, \tag{14}$$

and for z_0 ,

$$0 \approx -A^2 Y - B^2 X - \frac{W_{-1}}{c_{-1}^2} T + \frac{W_0}{c_0^2} T_D. \tag{15}$$

Solving the three linear equations (12, 14, 15) in X, Y, Z we remain with

$$\frac{T}{W_{-1}} = \frac{T_D}{W_0}. \tag{16}$$

Therefore the redshift is:

$$z := \frac{T_D - T}{T} \approx \frac{W_0}{W_{-1}} - 1 = \frac{\sqrt{\frac{A^2}{a_{-1}^2} + \frac{B^2}{b_{-1}^2} + \frac{C^2}{c_{-1}^2}}}{\sqrt{\frac{A^2}{a_0^2} + \frac{B^2}{b_0^2} + \frac{C^2}{c_0^2}}} - 1. \tag{17}$$

This formula agrees with the redshift derived in Saunders (1969), Koivisto & Mota (2008b) and Fontanini et al. (2009).

4 Apparent luminosity

To compute the apparent luminosity of a supernova at \vec{x}_{-1} , let it send out a rectangular beam of photons. One corner of this sequence of infinitesimal rectangles is given by the initial direction $\dot{x}(p_{-1}) = A/a_{-1}^2$, $\dot{y}(p_{-1}) = B/b_{-1}^2$, $\dot{z}(p_{-1}) = C/c_{-1}^2$. As before this photon leaves the supernova at t_{-1} . Formally this initial direction defines a space-like vector $(0, A/a_{-1}^2, B/b_{-1}^2, C/c_{-1}^2) =: (0, \vec{v}_{-1})$ in the tangent space at (t_{-1}, \vec{x}_{-1}) .

The two adjacent corners are defined by light-like geodesics with initial directions $\vec{v}_{-1} + \vec{\epsilon}_{-1}$ and $\vec{v}_{-1} + \vec{\delta}_{-1}$ where

$$\vec{\epsilon}_{-1} := \epsilon \left(\frac{B}{a_{-1}b_{-1}}, \frac{-A}{a_{-1}b_{-1}}, 0 \right) \quad (18)$$

$$\vec{\delta}_{-1} := \delta \left(\frac{AC}{a_{-1}^2c_{-1}}, \frac{BC}{b_{-1}^2c_{-1}}, - \left(\frac{A^2}{a_{-1}^2c_{-1}} + \frac{B^2}{b_{-1}^2c_{-1}} \right) \right). \quad (19)$$

We assume that A and B are not both zero. The three vectors \vec{v}_{-1} , $\vec{\epsilon}_{-1}$ and $\vec{\delta}_{-1}$ are mutually orthogonal with respect to the metric (1). We take ϵ and δ dimensionless. Then \vec{v}_{-1} , $\vec{\epsilon}_{-1}$ and $\vec{\delta}_{-1}$ have units s^{-1} . Their norms $|\vec{v}_{-1}|$, $|\vec{\epsilon}_{-1}|$, $|\vec{\delta}_{-1}|$ with respect to the metric are however dimensionless. The solid angle in the rest frame of the supernova at \vec{x}_{-1} cut out by the rectangular beam is given by

$$\Omega_{-1} = \frac{|\vec{\epsilon}_{-1}| \cdot |\vec{\delta}_{-1}|}{4\pi |\vec{v}_{-1}|^2} = \frac{\epsilon\delta}{4\pi} W_{-1} \left(\frac{A^2}{a_{-1}^2} + \frac{B^2}{b_{-1}^2} \right). \quad (20)$$

On its way to the detector at \vec{x}_0 the rectangular beam gets deformed into a sequence of infinitesimal parallelograms. The final parallelogram is defined by two infinitesimal vectors $\vec{\epsilon}_0 := \vec{x}_0^\epsilon - \vec{x}_0$ and $\vec{\delta}_0 := \vec{x}_0^\delta - \vec{x}_0$, where \vec{x}_0^ϵ is the space part of the light-like geodesic with initial direction $\vec{v}_{-1} + \vec{\epsilon}_{-1}$ and likewise for δ . This final parallelogram is the effective surface of the detector and our task is to compute its area. We have

$$x_0^\epsilon = \int_{t_{-1}}^{t_0} \frac{A + \epsilon B \frac{a_{-1}}{b_{-1}}}{a^2} \left(\frac{\left(A + \epsilon B \frac{a_{-1}}{b_{-1}} \right)^2}{a^2} + \frac{\left(B - \epsilon A \frac{b_{-1}}{a_{-1}} \right)^2}{b^2} + \frac{C^2}{c^2} \right)^{-1/2} dt \quad (21)$$

$$\approx x_0 + \epsilon B \int_{t_{-1}}^{t_0} \frac{W}{a^2} \left\{ \frac{a_{-1}}{b_{-1}} - A^2 W^2 \left[\frac{a_{-1}}{b_{-1}} \frac{1}{a^2} - \frac{b_{-1}}{a_{-1}} \frac{1}{b^2} \right] \right\} dt + O(\epsilon^2), \quad (22)$$

$$y_0^\epsilon = \int_{t_{-1}}^{t_0} \frac{B - \epsilon A \frac{b_{-1}}{a_{-1}}}{b^2} \left(\frac{\left(A + \epsilon B \frac{a_{-1}}{b_{-1}} \right)^2}{a^2} + \frac{\left(B - \epsilon A \frac{b_{-1}}{a_{-1}} \right)^2}{b^2} + \frac{C^2}{c^2} \right)^{-1/2} dt \quad (23)$$

$$\approx y_0 + \epsilon A \int_{t_{-1}}^{t_0} \frac{W}{b^2} \left\{ \frac{-b_{-1}}{a_{-1}} - B^2 W^2 \left[\frac{a_{-1}}{b_{-1}} \frac{1}{a^2} - \frac{b_{-1}}{a_{-1}} \frac{1}{b^2} \right] \right\} dt + O(\epsilon^2) \quad (24)$$

$$z_0^\epsilon = \int_{t_{-1}}^{t_0} \frac{C}{c^2} \left(\frac{\left(A + \epsilon B \frac{a_{-1}}{b_{-1}} \right)^2}{a^2} + \frac{\left(B - \epsilon A \frac{b_{-1}}{a_{-1}} \right)^2}{b^2} + \frac{C^2}{c^2} \right)^{-1/2} dt \quad (25)$$

$$\approx z_0 - \epsilon ABC \int_{t_{-1}}^{t_0} \frac{W^3}{c^2} \left[\frac{a_{-1}}{b_{-1}} \frac{1}{a^2} - \frac{b_{-1}}{a_{-1}} \frac{1}{b^2} \right] dt + O(\epsilon^2). \quad (26)$$

Similarly, one computes the components in δ and obtains to first order in ϵ and δ :

$$\vec{\epsilon}_0 \approx \epsilon \begin{pmatrix} B \int_{t_{-1}}^{t_0} \frac{W}{a^2} \left\{ \frac{a_{-1}}{b_{-1}} - A^2 W^2 \left[\frac{a_{-1}}{b_{-1}} \frac{1}{a^2} - \frac{b_{-1}}{a_{-1}} \frac{1}{b^2} \right] \right\} dt \\ A \int_{t_{-1}}^{t_0} \frac{W}{b^2} \left\{ \frac{-b_{-1}}{a_{-1}} - B^2 W^2 \left[\frac{a_{-1}}{b_{-1}} \frac{1}{a^2} - \frac{b_{-1}}{a_{-1}} \frac{1}{b^2} \right] \right\} dt \\ -ABC \int_{t_{-1}}^{t_0} \frac{W^3}{c^2} \left[\frac{a_{-1}}{b_{-1}} \frac{1}{a^2} - \frac{b_{-1}}{a_{-1}} \frac{1}{b^2} \right] dt \end{pmatrix}, \quad (27)$$

$$\vec{\delta}_0 \approx \delta \begin{pmatrix} \frac{AC}{c_{-1}} \int_{t_{-1}}^{t_0} \frac{W}{a^2} \left\{ 1 - W^2 \left[\frac{A^2}{a^2} + \frac{B^2}{b^2} - \frac{c_{-1}^2}{c^2} \left(\frac{A^2}{a_{-1}^2} + \frac{B^2}{b_{-1}^2} \right) \right] \right\} dt \\ \frac{BC}{c_{-1}} \int_{t_{-1}}^{t_0} \frac{W}{b^2} \left\{ 1 - W^2 \left[\frac{A^2}{a^2} + \frac{B^2}{b^2} - \frac{c_{-1}^2}{c^2} \left(\frac{A^2}{a_{-1}^2} + \frac{B^2}{b_{-1}^2} \right) \right] \right\} dt \\ - \int_{t_{-1}}^{t_0} \frac{W}{c^2} \left\{ c_{-1} \left(\frac{A^2}{a_{-1}^2} + \frac{B^2}{b_{-1}^2} \right) + \frac{C^2}{c_{-1}} W^2 \left[\frac{A^2}{a^2} + \frac{B^2}{b^2} - \frac{c_{-1}^2}{c^2} \left(\frac{A^2}{a_{-1}^2} + \frac{B^2}{b_{-1}^2} \right) \right] \right\} dt \end{pmatrix}.$$

Note that in contrast to our definitions at t_{-1} , the vectors $\vec{\epsilon}_0$ and $\vec{\delta}_0$ are dimensionless and their norms $|\vec{\epsilon}_0|$, $|\vec{\delta}_0|$ with respect to the metric carry seconds.

To first order in ϵ and δ these two vectors are orthogonal to \vec{v}_0 with respect to the metric (1):

$$\vec{\epsilon}_0 \cdot \vec{v}_0 \approx \vec{\delta}_0 \cdot \vec{v}_0 \approx 0. \quad (28)$$

Therefore the effective area is

$$S_0 \approx |\vec{\epsilon}_0 \wedge \vec{\delta}_0|, \quad (29)$$

where the vector product is computed with the metric (1). Finally the apparent luminosity is:

$$\ell = L \frac{\Omega_{-1}}{S_0} \left(\frac{W_{-1}}{W_0} \right)^2, \quad (30)$$

where L denotes the absolute luminosity of the standard candle, that we suppose to be radiating isotropically in its rest frame. Note that in the apparent luminosity ϵ and δ cancel.

Our formula disagrees with the one derived in eight lines by Koivisto & Mota (2008b):

$$\ell = \frac{L}{4\pi} \left[\int_{t_{-1}}^{t_0} (A^2 a^2 + B^2 b^2 + C^2 c^2)^{-1/2} dt \right]^{-2} \left(\frac{W_{-1}}{W_0} \right)^2 \quad (31)$$

(in our notations and using their normalisations: $a_0 = b_0 = c_0 = 1 = (A^2 + B^2 + C^2)^{1/2}$). If the photon moves in a principle direction, say $B = C = 0$, then Koivisto and Mota's apparent luminosity does not distinguish the Minkowskian metric, $a = b = c = 1$ s, from the one expanding in the x and y directions, say $a = b = \exp(Ht)$ s, $c = 1$ s. This is not compatible with the drift of luminous sources.

Our formula agrees with the one derived by Saunders (1969):

$$\ell = \frac{L}{4\pi} \frac{W_{-1}^5}{a_{-1} b_{-1} c_{-1} \Delta W_0^4}, \quad (32)$$

with:

$$I_x := - \int_{t_{-1}}^{t_0} \frac{W^3}{b^2 c^2} dt, \quad I_y := - \int_{t_{-1}}^{t_0} \frac{W^3}{c^2 a^2} dt, \quad I_z := - \int_{t_{-1}}^{t_0} \frac{W^3}{a^2 b^2} dt, \quad (33)$$

(compare with equations (13)) and $\Delta := A^2 I_y I_z + B^2 I_z I_x + C^2 I_x I_y$.

5 Einstein's equations

To keep things simple, we solve Einstein's equations with a positive cosmological constant Λ and dust whose mass density is denoted as usual by $\rho(t)$:

$$\text{Ric}_{\mu\nu} - \frac{1}{2} R g_{\mu\nu} = \Lambda g_{\mu\nu} + 8\pi G \rho \delta^0_\mu \delta^0_\nu. \quad (34)$$

Defining the Hubble parameters

$$H_x := \frac{a'}{a}, \quad H_y := \frac{b'}{b}, \quad H_z := \frac{c'}{c}, \quad \text{with} \quad ' := \frac{d}{dt}, \quad (35)$$

we have the following differential system:

$$\begin{aligned} (a) \quad & H'_x + H'_y + H_x^2 + H_y^2 + H_x H_y = \Lambda, \\ (b) \quad & H'_y + H'_z + H_y^2 + H_z^2 + H_y H_z = \Lambda, \\ (c) \quad & H'_z + H'_x + H_z^2 + H_x^2 + H_z H_x = \Lambda, \\ (d) \quad & H_x H_y + H_y H_z + H_z H_x = \Lambda + 8\pi G \rho. \end{aligned} \quad (36)$$

to which we may add the covariant energy-momentum conservation which integrates to

$$\rho(t) = \frac{r_*}{V(t)} \quad \text{with} \quad V(t) := a(t)b(t)c(t). \quad (37)$$

Here $r_* =: \rho_0 a_0 b_0 c_0$ is an integration constant.

5.1 The isotropic case

Let us observe that if we take $a = b = c$ we do recover Friedman's equations in the form

$$2H' + 3H^2 = \Lambda, \quad 3H^2 = \Lambda + 8\pi G \rho, \quad H := \frac{a'}{a}. \quad (38)$$

For positive Λ we integrate the first equation in H and obtain a bifurcation:

$$\begin{aligned} \Lambda/(3H^2) < 1 : \quad & H = \sqrt{\frac{\Lambda}{3}} \coth(u/2), \\ \Lambda/(3H^2) > 1 : \quad & H = \sqrt{\frac{\Lambda}{3}} \tanh(u/2), \end{aligned} \quad (39)$$

where $u := \sqrt{3\Lambda}(t-t_*)$ and t_* is an integration constant. Writing the scale factor $a = a_* V^{1/3}$ we have

$$\begin{aligned} \Lambda/(3H^2) < 1 : \quad & \frac{V}{V_0} = +\frac{4\pi G\rho_0}{\Lambda}(\cosh u - 1), \\ \Lambda/(3H^2) > 1 : \quad & \frac{V}{V_0} = -\frac{4\pi G\rho_0}{\Lambda}(\cosh u + 1). \end{aligned} \quad (40)$$

The bifurcation point yields the singular solution $H = \sqrt{\Lambda/3}$, for which the matter density vanishes, $\rho = 0$, by the second Friedman equation (38). The second branch, $\Lambda/(3H^2) > 1$, has negative matter density and no conventional physical interpretation.

For negative cosmological constant, $\Lambda < 0$, there is no bifurcation and we get

$$H = -\sqrt{\frac{|\Lambda|}{3}} \tan(u/2), \quad \frac{V}{V_0} = \frac{4\pi G\rho_0}{|\Lambda|} (1 + \cos u). \quad (41)$$

5.2 Integration of the Einstein equations

Let us begin with the first three equations: taking the difference between equations (a) and (b) we have

$$\frac{(H_y - H_x)'}{(H_y - H_x)} = -H_x - H_y - H_z = -\frac{V'}{V} \implies H_y = H_x + \frac{L}{V}. \quad (42)$$

The same treatment applied to the equations (a) and (c) gives

$$\frac{(H_z - H_x)'}{(H_z - H_x)} = -H_x - H_y - H_z = -\frac{V'}{V} \implies H_z = H_x + \frac{M}{V}. \quad (43)$$

In this step we got two new integrations constants L and M . Combining equations (b) and (c) gives no new relation.

Inserting the previous relations into equations (a), (b) and (c) we get three first order differential equations mixing H_x and V :

$$\begin{aligned} (a') \quad & 2H'_x + 3H_x^2 + \frac{3L}{V}H_x + \frac{L^2 - LV'}{V^2} = \Lambda, \\ (b') \quad & 2H'_x + 3H_x^2 + \frac{3(L+M)}{V}H_x + \frac{L^2 + M^2 + LM - (L+M)V'}{V^2} = \Lambda, \\ (c') \quad & 2H'_x + 3H_x^2 + \frac{3M}{V}H_x + \frac{M^2 - MV'}{V^2} = \Lambda. \end{aligned} \quad (44)$$

Subtracting (a') from (b') or (a') from (c') yields a single relation for H_x ,

$$H_x = \frac{V'}{3V} - \frac{L+M}{3V} \quad (45)$$

which, upon use of (42) and (43), implies

$$H_y = \frac{V'}{3V} + \frac{2L-M}{3V}, \quad H_z = \frac{V'}{3V} + \frac{-L+2M}{3V}. \quad (46)$$

We are left with (a') involving only the function $V(t)$. It reads

$$2V V'' - (V')^2 - 3\Lambda V^2 + \sigma^2 = 0, \quad \sigma^2 := L^2 - LM + M^2 \geq 0, \quad (47)$$

and is readily integrated once:

$$(V')^2 = \sigma^2 + 2EV + 3\Lambda V^2 \quad (48)$$

where E is a new integration constant.

It remains just to check the last equation (36) (d) : the computation gives the very simple relation

$$E = 12\pi G r_* . \quad (49)$$

The solution for the scale factors $a(t)$, $b(t)$, $c(t)$ is then obtained in the following steps:

1. First, compute the volume $V(t)$ by solving

$$(V')^2 = \sigma^2 + 24\pi G r_* V + 3\Lambda V^2, \quad \sigma^2 := L^2 - LM + M^2 \geq 0, \quad \Lambda > 0. \quad (50)$$

2. Deduce the Hubble parameters H_x , H_y , H_z from equations (45) and (46).

3. Finally integrate the Hubble parameters (35) and obtain the scale factors a , b , c .

Let us begin by integrating equation (50),

$$\frac{dV}{\sqrt{\sigma^2/3\Lambda + 2rV + V^2}} = \pm \sqrt{3\Lambda} dt, \quad r := \frac{4\pi G r_*}{\Lambda} \quad (51)$$

taking, without loss of generality, the positive sign. It is convenient to define

$$\xi := \sqrt{\frac{\Lambda}{3}} \frac{\sigma}{4\pi G r_*} > 0, \quad (52)$$

in order to write

$$\sigma^2/3\Lambda + 2rV + V^2 = (V+r)^2 - r^2(1-\xi^2). \quad (53)$$

The integration of (51) is then obvious for $\xi = 1$ and in the other cases the changes of variables

$$\xi < 1 : \quad V+r = r\sqrt{1-\xi^2} \cosh u, \quad \xi > 1 : \quad V+r = r\sqrt{\xi^2-1} \sinh u, \quad (54)$$

give easily the function V , which exhibits a bifurcation parametrized by ξ :

$$\begin{aligned} \xi < 1 & : & V &= \frac{4\pi G r_*}{\Lambda} \left(\sqrt{1-\xi^2} \cosh u - 1 \right), \\ \xi = 1 & : & V &= \frac{4\pi G r_*}{\Lambda} (e^u - 1), \\ \xi > 1 & : & V &= \frac{4\pi G r_*}{\Lambda} \left(\sqrt{\xi^2-1} \sinh u - 1 \right), \end{aligned} \quad (55)$$

with $u = \sqrt{3\Lambda}(t - t_*)$ as before. The very simple structure of these functions may be understood by differentiating equation (50) which gives the linear equation

$$V'' - 3\Lambda V = 12\pi Gr_*. \quad (56)$$

For the third step, we show the computation only for $a(t)$ with $\xi < 1$. We start from equation (45),

$$H_x = \frac{a'}{a} = \frac{V'}{3V} - \frac{(L+M)}{3V}, \quad (57)$$

and integrate:

$$a(t) = a_* V^{1/3} \exp\left(-\frac{(L+M)}{3} \int \frac{dt}{V}\right). \quad (58)$$

We need to fix the sign of V , which is positive. Therefore $u > \text{Artanh } \xi$. We have

$$\int \frac{dt}{V} = \frac{\xi}{\sigma\sqrt{1-\xi^2}} \int \frac{du}{\cosh u - 1/\sqrt{1-\xi^2}} = \frac{2}{\sigma} \xi \sqrt{1-\xi^2} \int \frac{e^u du}{\left(\sqrt{1-\xi^2} e^u - 1\right)^2 - \xi^2}, \quad (59)$$

and the change of variables

$$v = \frac{1}{\xi} \left(\sqrt{1-\xi^2} e^u - 1\right) > 1, \quad (60)$$

yields

$$\int \frac{dt}{V} = \frac{2}{\sigma} \int \frac{dv}{v^2 - 1} = \frac{1}{\sigma} \ln \frac{e^u - w}{e^u - 1/w}, \quad \text{with } w := \exp \text{Artanh } \xi = \sqrt{\frac{1+\xi}{|1-\xi|}}. \quad (61)$$

The computations are similar for the other scale factors. With the definitions

$$s_1 := -\frac{L+M}{3\sigma}, \quad s_2 := \frac{2L-M}{3\sigma}, \quad (62)$$

we obtain

$$a(t) = a_* V(t)^{1/3} R(t)^{s_1}, \quad b(t) = b_* V(t)^{1/3} R(t)^{s_2}, \quad c(t) = \frac{V(t)}{a(t)b(t)}, \quad (63)$$

where a_* and b_* are integration constants and R is the strictly positive function of time defined by

$$\begin{cases} \xi < 1 & : & R(t) := \frac{e^u - w}{e^u - 1/w}, & u > \text{Artanh } \xi, \\ \xi = 1 & : & R(t) := 1 - e^{-u}, & u > 0, \\ \xi > 1 & : & R(t) := \frac{e^u - w}{e^u + 1/w}, & u > \text{Artanh}(1/\xi). \end{cases} \quad (64)$$

A few remarks are in order:

- As time grows, the anisotropy of the Universe fades away since $R \rightarrow 1$. This is a well-known property of Bianchi I cosmologies. In particular, equations (42) and (43) show that this fading is driven by increasing volume V .
- If we choose $t_* = -(\text{Artanh } \xi)/\sqrt{3\Lambda}$ in the first case, $\xi < 1$, then the big bang occurs at $t = 0$.
- The discussed solution is usually attributed to Saunders (1969). His field equations are

$$\begin{aligned}
H'_x + \frac{1}{3} H_x(H_x + H_y + H_z) &= \Lambda + 4\pi G\rho, \\
H'_y + \frac{1}{3} H_y(H_x + H_y + H_z) &= \Lambda + 4\pi G\rho, \\
H'_z + \frac{1}{3} H_z(H_x + H_y + H_z) &= \Lambda + 4\pi G\rho, \\
H_x H_y + H_y H_z + H_z H_x &= \Lambda + 8\pi G\rho.
\end{aligned} \tag{65}$$

In the isotropic limit where $H_x = H_y = H_z =: H$ we obtain

$$H' + H^2 = \Lambda + 4\pi G\rho \quad 3H^2 = \Lambda + 8\pi G\rho. \tag{66}$$

Eliminating ρ in the first equation by using the second equation they read

$$2H' - H^2 = \Lambda \quad 3H^2 = \Lambda + 8\pi G\rho \tag{67}$$

and are at variance with Friedman's equations (38).

- Note that in the isotropic limit, σ goes to zero and some intermediate results, e.g. equation (59), in our derivation of the solutions to Einstein's equations are singular. One way to avoid these singularities is to take the limit in two steps with the intermediate step being the ellipsoid of revolution. In any case, our final solutions, the scale factors (63), have a well defined limit.
- For completeness we also indicate the case of negative cosmological constant. Defining this time

$$r := \frac{4\pi Gr_*}{|\Lambda|} \quad \xi := \sqrt{\frac{|\Lambda|}{3}} \frac{\sigma}{4\pi Gr_*}, \tag{68}$$

we can write the differential equation (50) for V in the form

$$\frac{dV}{\sqrt{-(V+r)^2 + r^2(1-\xi^2)}} = \sqrt{3|\Lambda|} dt \tag{69}$$

showing that there is no bifurcation since now ξ must be smaller than one for V to remain real. The change of variables

$$V + r = r\sqrt{1-\xi^2} \sin u \tag{70}$$

gives easily

$$\frac{V}{V_0} = -\frac{4\pi G\rho_0}{|\Lambda|} \left(1 - \sqrt{1 - \xi^2} \sin u\right) < 0 \quad u = \sqrt{3|\Lambda|} (t - t_*), \quad (71)$$

and if one defines

$$s_1 = 2 \frac{L + M}{3\sigma}, \quad s_2 = -2 \frac{2L - M}{3\sigma}, \quad (72)$$

the scale factors are

$$a(t) = a_* V(t)^{1/3} \exp[s_1 \arctan R(t)], \quad (73)$$

$$b(t) = b_* V(t)^{1/3} \exp[s_2 \arctan R(t)], \quad c(t) = \frac{V(t)}{a(t)b(t)}, \quad (74)$$

with

$$R(t) = \frac{\arctan(u/2) - \sqrt{1 - \xi^2}}{\xi}. \quad (75)$$

6 Small eccentricities

No drift in the positions of quasars or galaxies has been observed today. We therefore assume that the three scale factors a , b and c differ only by small amounts:

$$b(t) =: a(t) [1 + \beta(t)], \quad c(t) =: a(t) [1 + \eta(t)], \quad \beta, \eta \ll 1. \quad (76)$$

As explained after equation (6), we may set $\beta(t_0) = \eta(t_0) = 0$ without loss of generality.

6.1 Kinematics

In the following we keep only leading terms in ϵ , δ and β , η , and continue using \approx to indicate this approximation.

Let us introduce the abbreviations $N^2 := A^2 + B^2 + C^2 = 1 \text{ s}^2$, $\chi := \int_{t_{-1}}^{t_0} dt/a$, $\bar{\beta} := \chi^{-1} \int_{t_{-1}}^{t_0} \beta dt/a$ and $\bar{\eta} := \chi^{-1} \int_{t_{-1}}^{t_0} \eta dt/a$. Note that χ is the dimensionless comoving geodesic “distance” between the supernova emitting the photon and the Earth. In these notations the kinematics reads:

$$W \approx \frac{a}{N} \left[1 + \frac{B^2}{N^2} \beta + \frac{C^2}{N^2} \eta \right], \quad (77)$$

$$z + 1 = \frac{W_0}{W_{-1}} \approx \frac{a_0}{a_{-1}} \left[1 - \frac{B^2}{N^2} \beta_{-1} - \frac{C^2}{N^2} \eta_{-1} \right], \quad (78)$$

$$\epsilon_{0x} \approx \epsilon \frac{B}{N} \chi \left[1 - \left(1 - 2 \frac{A^2}{N^2} \right) \beta_{-1} + \left(-2 + 3 \frac{B^2}{N^2} + 2 \frac{C^2}{N^2} \right) \bar{\beta} + \frac{C^2}{N^2} \bar{\eta} \right], \quad (79)$$

$$\epsilon_{0y} \approx -\epsilon \frac{A}{N} \chi \left[1 + \left(1 - 2 \frac{\beta^2}{N^2} \right) \beta_{-1} + \left(-2 + 3 \frac{B^2}{N^2} \right) \bar{\beta} + \frac{C^2}{N^2} \bar{\eta} \right], \quad (80)$$

$$\epsilon_{0z} \approx -\epsilon \frac{ABC}{N^3} \chi \left[-2 \beta_{-1} + 2 \bar{\beta} \right], \quad (81)$$

$$\delta_{0x} \approx \delta \frac{AC}{Na_{-1}} \chi \left[1 - 2 \frac{B^2}{N^2} \beta_{-1} + 3 \frac{B^2}{N^2} \bar{\beta} + \left(1 - 2 \frac{C^2}{N^2} \right) \eta_{-1} + \left(-2 + 3 \frac{C^2}{N^2} \right) \bar{\eta} \right], \quad (82)$$

$$\delta_{0y} \approx \delta \frac{BC}{Na_{-1}} \chi \left[1 - 2 \frac{B^2}{N^2} \beta_{-1} + \left(-2 + 3 \frac{B^2}{N^2} \right) \bar{\beta} + \left(1 - 2 \frac{C^2}{N^2} \right) \eta_{-1} + \left(-2 + 3 \frac{C^2}{N^2} \right) \bar{\eta} \right], \quad (83)$$

$$\delta_{0z} \approx -\delta \frac{A^2 + B^2}{Na_{-1}} \chi \left[1 - 2 \frac{B^2}{N^2} \beta_{-1} + \frac{B^2}{N^2} \left(1 - 2 \frac{C^2}{A^2 + B^2} \right) \bar{\beta} + \left(1 - 2 \frac{C^2}{N^2} \right) \eta_{-1} + \left(-2 + 3 \frac{C^2}{N^2} \right) \bar{\eta} \right], \quad (84)$$

$$S_0 \approx \epsilon \delta \frac{A^2 + B^2}{N} \frac{a_0^2}{a_{-1}} \chi^2 \cdot \left[1 + \left(\frac{A^2}{N^2} - 3 \frac{B^2}{N^2} + \frac{A^2 - B^2}{A^2 + B^2} \frac{C^2}{N^2} \right) \beta_{-1} - 2 \left(1 - 2 \frac{B^2}{N^2} \right) \bar{\beta} + \left(1 - 2 \frac{C^2}{N^2} \right) \eta_{-1} - 2 \left(1 - 2 \frac{C^2}{N^2} \right) \bar{\eta} \right], \quad (85)$$

$$\Omega_{-1} \approx \frac{\epsilon \delta}{4\pi} \frac{A^2 + B^2}{Na_{-1}} \left[1 + \left(\frac{B^2}{N^2} - 2 \frac{B^2}{A^2 + B^2} \right) \beta_{-1} + \frac{C^2}{N^2} \eta_{-1} \right], \quad (86)$$

$$\ell \approx \frac{L}{4\pi \chi^2 a_0^2} \frac{a_{-1}^2}{a_0^2} \left[1 - \left(1 - 5 \frac{B^2}{N^2} \right) \beta_{-1} + 2 \left(1 - 2 \frac{B^2}{N^2} \right) \bar{\beta} - \left(1 - 5 \frac{C^2}{N^2} \right) \eta_{-1} + 2 \left(1 - 2 \frac{C^2}{N^2} \right) \bar{\eta} \right]. \quad (87)$$

In linear approximation, the formula by Koivisto & Mota (2008b) reads:

$$\ell \approx \frac{L}{4\pi \chi^2 a_0^2} \frac{a_{-1}^2}{a_0^2} \left[1 + 2 \frac{B^2}{N^2} \beta_{-1} + 2 \frac{B^2}{N^2} \bar{\beta} + 2 \frac{C^2}{N^2} \eta_{-1} + 2 \frac{C^2}{N^2} \bar{\eta} \right].$$

6.2 Dynamics

For the dynamics we will not only suppose $\beta(t)$ and $\eta(t)$ small, but also $\beta'(t)/\sqrt{3\Lambda}$ and $\eta'(t)/\sqrt{3\Lambda}$ small and indicate by \approx the leading approximation in all small quantities.

From equations (42) and (43) we get:

$$L = V(H_y - H_x) = V \left(\frac{b'}{b} - \frac{a'}{a} \right) = V \frac{\beta'}{1 + \beta} \approx V \beta' = V_0 \beta'_0, \quad (88)$$

$$M = V(H_z - H_x) = V \left(\frac{c'}{c} - \frac{a'}{a} \right) = V \frac{\eta'}{1 + \eta} \approx V \eta' = V_0 \eta'_0. \quad (89)$$

By its definition (52), the bifurcation parameter becomes

$$\xi = \frac{2}{g} \sqrt{\frac{\beta_0'^2 - \beta_0' \eta_0' + \eta_0'^2}{3\Lambda}} \ll 1, \quad \text{with} \quad g := \frac{8\pi G \rho_0}{\Lambda}, \quad (90)$$

showing that we are in the first case of the bifurcation. Linearising the scale factors in this case we get:

$$\frac{a}{a_0} \approx \left(\frac{g}{2} \right)^{1/3} (\cosh u - 1)^{1/3} \left[1 + \frac{4}{3} \frac{\beta_0' + \eta_0'}{g \sqrt{3\Lambda}} \left\{ \frac{1}{e^u - 1} - \frac{1}{2} (\sqrt{g+1} - 1) \right\} \right], \quad (91)$$

$$\frac{b}{b_0} \approx \left(\frac{g}{2} \right)^{1/3} (\cosh u - 1)^{1/3} \left[1 + \frac{4}{3} \frac{-2\beta_0' + \eta_0'}{g \sqrt{3\Lambda}} \left\{ \frac{1}{e^u - 1} - \frac{1}{2} (\sqrt{g+1} - 1) \right\} \right], \quad (92)$$

$$\frac{c}{c_0} \approx \left(\frac{g}{2} \right)^{1/3} (\cosh u - 1)^{1/3} \left[1 + \frac{4}{3} \frac{\beta_0' - 2\eta_0'}{g \sqrt{3\Lambda}} \left\{ \frac{1}{e^u - 1} - \frac{1}{2} (\sqrt{g+1} - 1) \right\} \right], \quad (93)$$

and for the eccentricities:

$$\beta \approx -4 \frac{\beta_0'}{g \sqrt{3\Lambda}} \left\{ \frac{1}{e^u - 1} - \frac{1}{2} (\sqrt{g+1} - 1) \right\}, \quad (94)$$

$$\eta \approx -4 \frac{\eta_0'}{g \sqrt{3\Lambda}} \left\{ \frac{1}{e^u - 1} - \frac{1}{2} (\sqrt{g+1} - 1) \right\}. \quad (95)$$

The consistency of these relations can be checked by computing its derivative with respect to time t and by using equation (55) with $\xi = 0$ and $t = t_0$:

$$g (\cosh u_0 - 1) = 2. \quad (96)$$

Next we solve the redshift, equation (78),

$$z + 1 \approx \frac{a_0}{a(t)} \left[1 - \frac{B^2}{N^2} \beta(t) - \frac{C^2}{N^2} \eta(t) \right], \quad (97)$$

for the departure time of the photon at the supernova. To alleviate notations, this departure time t_{-1} is now simply written t or will be omitted. In linear approximation we have:

$$u = \sqrt{3\Lambda} (t - t_*) \approx u_F + \frac{2}{g \sqrt{3\Lambda}} \left[\left(3 \frac{B^2}{N^2} - 1 \right) \beta'_0 + \left(3 \frac{C^2}{N^2} - 1 \right) \eta'_0 \right] \frac{D}{\sqrt{g(z+1)^3 + 1}}, \quad (98)$$

$$\text{with } u_F := \text{Arcosh} \left[\frac{2}{g(z+1)^3} + 1 \right] \quad \text{and} \quad D := \sqrt{g(z+1)^3 + 1} - \sqrt{g+1} \quad (99)$$

For the apparent luminosity,

$$\begin{aligned} \ell \approx & \frac{L}{4\pi\chi^2 a_0^2} \frac{a_{-1}^2}{a_0^2} \left[1 - \left(1 - 5 \frac{B^2}{N^2} \right) \beta_{-1} + 2 \left(1 - 2 \frac{B^2}{N^2} \right) \bar{\beta} \right. \\ & \left. - \left(1 - 5 \frac{C^2}{N^2} \right) \eta_{-1} + 2 \left(1 - 2 \frac{C^2}{N^2} \right) \bar{\eta} \right], \end{aligned} \quad (100)$$

we need the geodesic distance χ , the scale factor a , and the eccentricities β and η , all four at the time of departure of the photon from the supernova and we need the eccentricities averaged over the time of flight of the photon between the supernova and the Earth $\bar{\beta}$ and $\bar{\eta}$, all six as functions of redshift in linear approximation. Let us denote isotropic quantities, $\beta = \eta = 0$, with a subscript \cdot_F for Friedman:

$$\chi_F = \frac{I}{a_0} \sqrt{\frac{3}{\Lambda}}, \quad a_F = \frac{a_0}{z+1}, \quad \ell_F = \frac{L}{4\pi} \frac{\Lambda}{3I^2(z+1)^2}, \quad H_F(z) = \sqrt{\frac{\Lambda}{3}} \sqrt{g(z+1)^3 + 1}, \quad (101)$$

with the elliptic integral, cf appendix 1:

$$I(z) := \int_0^z \frac{d\tilde{z}}{\sqrt{g(\tilde{z}+1)^3 + 1}} = \sqrt{\frac{\Lambda}{3}} \int_0^z \frac{d\tilde{z}}{H_F(\tilde{z})}. \quad (102)$$

With these notations we can write:

$$\chi \approx \chi_F \left[1 + \frac{2}{3} \frac{\beta'_0}{g\sqrt{3\Lambda}} \left\{ \sqrt{g+1} - \frac{z}{I} + \left(1 - 3 \frac{B^2}{N^2} \right) \frac{z+1}{I} \frac{D}{\sqrt{g(z+1)^3 + 1}} \right\} \right] \quad (103)$$

$$\left. \frac{2}{3} \frac{\eta'_0}{g\sqrt{3\Lambda}} \left\{ \sqrt{g+1} - \frac{z}{I} + \left(1 - 3 \frac{C^2}{N^2} \right) \frac{z+1}{I} \frac{D}{\sqrt{g(z+1)^3 + 1}} \right\} \right], \quad (104)$$

$$a \approx a_F \left[1 + \frac{2}{g\sqrt{3\Lambda}} \left(\frac{B^2}{N^2} \beta'_0 + \frac{C^2}{N^2} \eta'_0 \right) D \right], \quad (105)$$

$$\beta \approx -2 \frac{\beta'_0}{g\sqrt{3\Lambda}} D, \quad \bar{\beta} \approx -2 \frac{\beta'_0}{g\sqrt{3\Lambda}} \left\{ \frac{z}{I} - \sqrt{g+1} \right\}, \quad (106)$$

$$\eta \approx -2 \frac{\eta'_0}{g\sqrt{3\Lambda}} D, \quad \bar{\eta} \approx -2 \frac{\eta'_0}{g\sqrt{3\Lambda}} \left\{ \frac{z}{I} - \sqrt{g+1} \right\}. \quad (107)$$

Finally, the apparent luminosity as a function of redshift is in linear approximation:

$$\ell \approx \ell_F \left[1 - \frac{2}{\sqrt{3\Lambda}} \left\{ \left(1 - 3 \frac{B^2}{N^2} \right) \beta'_0 + \left(1 - 3 \frac{C^2}{N^2} \right) \eta'_0 \right\} Q \right], \quad (108)$$

$$Q := \frac{1}{3g} \left\{ 4 \left(\frac{z}{I} - \sqrt{g+1} \right) + \left(2 \frac{z+1}{I\sqrt{g(z+1)^3 + 1}} - 3 \right) D \right\}. \quad (109)$$

Note that for small redshift, we have

$$Q \approx \frac{1}{\sqrt{g+1}}, \quad (110)$$

$$\lim_{z \rightarrow 0} (z^2 \ell) \approx \frac{L}{4\pi} H_{F0}^2 \left[1 - \frac{2}{3} \left(1 - 3 \frac{B^2}{N^2} \right) \frac{\beta'_0}{H_{F0}} - \frac{2}{3} \left(1 - 3 \frac{C^2}{N^2} \right) \frac{\eta'_0}{H_{F0}} \right]. \quad (111)$$

Note also that Einstein's equations imply:

$$H_x \approx H_F - \frac{1}{3}\beta' - \frac{1}{3}\eta', \quad H_y \approx H_F + \frac{2}{3}\beta' - \frac{1}{3}\eta', \quad H_z \approx H_F - \frac{1}{3}\beta' + \frac{2}{3}\eta', \quad (112)$$

and

$$\Omega_m + \Omega_\Lambda = 1 + O(\beta, \eta)^2, \quad \text{with} \quad \Omega_m := \frac{8\pi G \rho_0}{3H_{F0}^2}, \quad \Omega_\Lambda := \frac{\Lambda}{3H_{F0}^2}. \quad (113)$$

We have two privileged perpendicular directions, the x - and z -axes. The y -axis is then determined up to a sign, which is irrelevant because of reflection invariance of the Bianchi I metric (1). We denote by $\theta \in [0, \pi]$ the angle of the incoming photon with the z -axis and by $\varphi \in [0, 2\pi)$ the angle between the projection of the incoming photon into the xy -plane and the x -axis:

$$A = N \cos \varphi \sin \theta, \quad (114)$$

$$B = N \sin \varphi \sin \theta, \quad (115)$$

$$C = N \cos \theta. \quad (116)$$

In these notations the apparent luminosity as a function of redshift reads:

$$\ell \approx \ell_F \left[1 + \frac{2}{\sqrt{3\Lambda}} \{ \beta'_0 (3 \sin^2 \varphi \sin^2 \theta - 1) + \eta'_0 (3 \cos^2 \theta - 1) \} Q \right], \quad (117)$$

with the isotropic apparent luminosity

$$\ell_F = \frac{L}{4\pi} \frac{\Lambda}{3I^2(z+1)^2}, \quad (118)$$

the elliptic integral

$$I(z) := \int_0^z \frac{d\tilde{z}}{\sqrt{g(\tilde{z}+1)^3+1}}, \quad g := \frac{8\pi G \rho_0}{\Lambda}, \quad (119)$$

and the auxiliary function

$$Q := \frac{1}{3g} \left\{ 4 \left(\frac{z}{I} - \sqrt{g+1} \right) + \left(2 \frac{z+1}{I\sqrt{g(z+1)^3+1}} - 3 \right) \left(\sqrt{g(z+1)^3+1} - \sqrt{g+1} \right) \right\}. \quad (120)$$

7 Data analysis

To confront the Bianchi I metric with data we use the type 1a supernovae Hubble diagram from the Union 2 sample (Amanullah et al. 2010) with 557 supernovae up to a redshift of 1.4 and the Joint Light curve Analysis (JLA) (Betoule et al. 2014) with 740 supernovae up to a redshift of 1.3. Note that 258 supernovae belong simultaneously to both samples. Supernovae celestial coordinates are obtained from the SIMBAD astronomical database.

For the Union 2 sample, published data are the supernovae magnitudes at maximum of luminosity corrected by time stretching of the light curve and color at maximum brightness. The associated statistical and systematic errors are provided by the full covariance matrix of supernovae magnitudes including correlations.

The JLA published data provide the observed uncorrected peak magnitudes (m_{peak}), time stretching ($X1$) and color (C) with the full statistical and systematic covariance matrix between all measurements including correlations between supernovae. The total likelihood or χ^2 is computed following the JLA paper prescription and a rewriting of the likelihood computation program provided by the COSMOMC package (Lewis & Bridle 2002). We choose to use the frequentist statistic (Amsler et al. 2008) based on χ^2 minimization. The MINUIT package is used to find the minimum and to compute errors with the second χ^2 derivative. All presented results are obtained after marginalization over nuisance parameters. The χ^2 expression reads:

$$\chi^2 = \Delta M^T V^{-1} \Delta M, \quad (121)$$

where ΔM is the vector of differences between reconstructed (m_r) and expected (m_e) magnitudes at maximum and V is the full covariance matrix including systematic errors. The reconstructed magnitude for JLA reads:

$$m_r = m_{\text{peak}} + \alpha_s X1 - \beta_c C, \quad (122)$$

where α_s and β_c are fitted simultaneously with the additional free parameters. The expected magnitude is written as $m_e(z) = m_s - 2.5 \log \ell(z)$ where m_s is a normalization parameter fitted to the data.

Let us define the three dimensionless Hubble stretch parameters today as

$$h_i := H_{i0}/H_{F0} - 1 \quad \text{for } i = x, y, z. \quad (123)$$

Using formula (112) they read:

$$h_x \approx -\frac{1}{3}(\beta'_0 + \eta'_0)/H_{F0}, \quad h_y \approx \frac{1}{3}(2\beta'_0 - \eta'_0)/H_{F0}, \quad h_z \approx \frac{1}{3}(-\beta'_0 + 2\eta'_0)/H_{F0}, \quad (124)$$

and verify $h_x + h_y + h_z = 0$.

The apparent luminosity $\ell(z)$ is computed with equation (117) rewritten in terms of the two Hubble stretch parameters h_z, h_x .

$$\ell \approx \ell_F \left[1 + \frac{2}{\sqrt{\Omega_\Lambda}} \{h_z (\cos^2 \theta - \sin^2 \varphi \sin^2 \theta) + h_x \cos 2\varphi \sin^2 \theta\} Q \right], \quad (125)$$

We search for preferred directions by scanning the celestial sphere in steps of 1 degree in right ascension and declination. For each direction (r_z, d_z) assumed to be the z direction, we minimize the χ^2 over all other free parameters including Ω_m and assuming a flat Universe. The minimum χ^2 in the (r_z, d_z) plane defines the privileged direction as well as the confidence level contours.

Because of the huge number of χ^2 to minimize and because the JLA sample requires many large matrix inversions, the following analysis represents more than 100 000 hours of computing time on a single CPU. To speed up the processing, we use the EGEE (Enabling Grids for E-science) datagrid facility with the DIRAC web interface (Tsaregorodtsev et al. 2008).

7.1 Bianchi I with axial symmetry

We first look for a unique preferred direction along \vec{u}_z . For the case of axial symmetry, we take the Hubble stretch parameters in the x - and y -directions to be equal: $h_x = h_y = -h_z/2$. Then equation (125) simplifies to:

$$\ell \approx \ell_F \left[1 + \frac{1}{\sqrt{\Omega_\Lambda}} \{h_z (3 \cos^2 \theta - 1)\} Q \right], \quad (126)$$

For each celestial direction \vec{u}_z , we define θ to be the angle between \vec{u}_z and the direction of the incoming photons from the supernovae. The isotropic apparent luminosity is computed by rewriting formula (118) as:

$$\ell_F = \frac{LH_{F0}^2}{4\pi} \frac{1 - \Omega_m}{I(z)^2(z+1)^2} \quad (127)$$

The unknown constant term $LH_{F0}^2/4\pi$ is absorbed into the fitted normalization parameter m_s . The elliptic integral $I(z)$ is computed numerically.

Figure 1 shows the confidence level contours with arbitrary color codes around the eigendirections on the celestial sphere for the Union 2 and JLA samples. The black points show the supernovae positions. Notice that the Bianchi I metric is symmetric under space reflections. We therefore expect two back-to-back eigendirections with the same eigenvalues, which is indeed the case. Figure 1 has two distinct eigendirections, a main one indicated by a gray speck and a secondary one in green. The full blue line is the galactic plane and the purple one corresponds to the plane orthogonal to the main eigendirection (gray speck). The statistical significance of the main eigendirection for the Union 2 sample is about 41% while it increases to 58% for JLA. The main eigendirections in the two samples are statistically compatible (Table 1). They are close to the galactic plane and almost orthogonal to the direction from the sun to the galactic center. For both samples, the Hubble stretch h_z is negative and at most 1.2σ away from zero.

In Figure 1 the green specks represent a secondary direction with a weaker statistical significance (30% and 35% confidence level for Union 2 and JLA respectively). They are in the plane orthogonal to the main direction (purple line). The Hubble stretch in this secondary direction has an opposite sign. Even though it is a weak statistical effect, data seem to call for

Sample	Union 2		JLA	
Direction	main	secondary	main	secondary
right ascension(°)	103 ± 58	169 ± 36	158 ± 29	160 ± 97
declination (°)	-56 ± 36	24 ± 35	-60 ± 11	-70 ± 50
galactic longitude (°)	88 ± 45	36 ± 87	106 ± 16	23 ± 41
galactic latitude (°)	22 ± 26	-68 ± 30	1 ± 10	19 ± 31
Hubble stretch in %	-1.1 ± 1.1	0.7 ± 0.9	-1.7 ± 1.3	0.5 ± 0.9
χ^2 Bianchi I	529.64	529.98	699.35	700.43
Ω_m	0.27 ± 0.04		0.29 ± 0.03	
χ^2 isotropic	530.71		701.3	

Table 1: Fit results (1σ errors) for Bianchi I with axial symmetry. We have used the invariance of the Bianchi I metric under space reflection to constrain the eigendirections to the hemispheres with right ascension or galactic longitude between 0° and 180° .

a second eigendirection. This feature is clearly observed in Figure 3 presenting our simulation program. As a possible consequence, the minimum χ^2 is not as good as one would expect from three additional degrees of freedom compared to the isotropic case. We conclude that there is some stress in the data when confronted to the Bianchi I with axial symmetry.

7.2 Tri-axial Bianchi I

The last remarks motivate us to extend the fit to the general Bianchi I metric with three distinct eigenvalues and three orthogonal eigenvectors.

As in the previous subsection we start with a first eigendirection \vec{u}_z defined by its celestial coordinates (r_z, d_z) :

$$\vec{u}_z := (\cos r_z \cos d_z, \sin r_z \cos d_z, \sin d_z) \quad (128)$$

We then construct an orthonormal basis $(\vec{v}_x, \vec{v}_y, \vec{v}_z = \vec{u}_z)$ as follows: We choose the second unit vector $\vec{v}_x := (\sin r_z, -\cos r_z, 0)$ orthogonal to \vec{v}_z . The third unit vector is then defined by: $\vec{v}_y := \vec{v}_z \wedge \vec{v}_x$.

The second eigendirection \vec{u}_x is obtained by rotating the vector \vec{v}_x by an angle γ around \vec{u}_z . The third eigendirection is completely fixed as well as the corresponding stretch parameters. The angle θ is the angle between \vec{u}_z and the direction of the incoming photons from the supernovae and φ is the angle between \vec{u}_x and the projection of the incoming photon into the (\vec{v}_x, \vec{v}_y) plane.

For each direction defined by its celestial coordinates we compute the χ^2 with formula (125) and minimize it with respect to the following set of free parameters: $m_s, \alpha_s, \beta_c, \Omega_m, h_z, h_x$ and γ .

Figure 2 shows the confidence level contours with arbitrary color codes around the eigendirections on the celestial sphere. The gray specks mark the three eigendirections in each hemisphere. They materialize the unit vectors \vec{u}_x, \vec{u}_y and \vec{u}_z . The main eigendirection has

by definition the largest Hubble stretch in absolute value and is given by \vec{u}_z . As in the axial case, this direction is close to the galactic plane (blue line). The two remaining eigendirections are contained in the plane orthogonal to the main eigendirection \vec{u}_z (purple curve). Blue specks within blue contours are regions where χ^2 is *maximum*. They correspond to the underprivileged regions that we expect on a sphere with several minima of χ^2 .

Table 2 summarizes the eigendirections and eigenvalues for the Union 2 and JLA supernovae samples. The main eigendirections \vec{u}_z of both samples are close to each other. And they are statistically compatible with the main eigendirection of the axially symmetric case. The main Hubble stretch h_z is negative with a maximum significance of 1.3σ . In the JLA sample, both secondary Hubble stretch parameters are very similar, which is compatible with the axial symmetry. The improvement in the minimum χ^2 compared to the isotropic case is of the order of 2 units which is still too low for four added degrees of freedom.

Sample	Union 2			JLA		
Direction	\vec{u}_x	\vec{u}_y	\vec{u}_z	\vec{u}_x	\vec{u}_y	\vec{u}_z
ascension($^\circ$)	142 ± 67	48 ± 59	126 ± 52	160 ± 30	34 ± 64	177 ± 56
declination($^\circ$)	33 ± 21	8 ± 32	-58 ± 21	28 ± 14	-20 ± 20	-65 ± 14
longitude($^\circ$)	12 ± 35	172 ± 51	91 ± 30	28 ± 28	18 ± 36	116 ± 25
latitude($^\circ$)	-47 ± 52	-41 ± 53	10 ± 20	-21 ± 60	69 ± 57	3 ± 11
stretch($\%$)	1.2 ± 1.1	0.3 ± 0.7	-1.5 ± 1.3	0.7 ± 1.0	1.1 ± 1.1	-1.8 ± 1.4
χ^2 Bianchi I	529.08			699.1		
Ω_m	0.27 ± 0.04			0.28 ± 0.04		
χ^2 isotropic	530.71			701.3		

Table 2: Fit results (1σ errors) for tri-axial Bianchi I. We have used the invariance of the Bianchi I metric under space reflection to constrain the eigendirections to the hemispheres with right ascension or galactic longitude between 0° and 180° .

7.3 Preliminary discussion

The largest Hubble stretch we find in absolute value is equal to $h_z = -1.8\%$ with a statistical significance of about 1.3σ . In the following sense, this corresponds to a pumpkin-like Universe in the future:

Consider a small, 2-dimensional, comoving sphere today, $t = t_0$, in a Bianchi I Universe with axial symmetry around the z -axis, $a(t) = b(t)$, and with negative Hubble stretch h_z . Recall that in our conventions $a(t_0) = b(t_0) = c(t_0)$. Then this sphere evolves with Einstein's equations in the future, $t > t_0$, into an oblate ellipsoid of revolution (pumpkin), $a(t) = b(t) > c(t)$. However, it comes from a prolate ellipsoid of revolution (rugby ball), $a(t) = b(t) < c(t)$ in the past, $t < t_0$. Indeed Einstein's equations imply that the Hubble stretches cannot change sign.

The main privileged direction is in all cases contained in the galactic plane and almost orthogonal to the direction between the sun and the galactic center. One is tempted to think

that we are just measuring our proper velocity around the galactic center. In principle, the observer’s proper velocity is already corrected for in the calibration of the data. Nevertheless, we will test the hypothesis of a forward-backward asymmetry. To this end, we split the supernovae of both samples into two hemispheres with respect to the main eigendirection \vec{u}_z , backward (\vec{u}_z^+) and forward (\vec{u}_z^-) corresponding respectively to the regions above and below the purple line in Figure 2. The number of supernovae per hemisphere is 338 (respectively 219) in the backward (respectively forward) hemisphere for Union 2 and 100 (respectively 640) for JLA.

Using the axially symmetric fitting procedure and fixing \vec{u}_z to the main direction as in Table 2, we find $h_z^+ = (1.3 \pm 2.1) \%$, $h_z^- = -(2.3 \pm 1.5) \%$ for Union 2 and $h_z^+ = (2.8 \pm 2.9) \%$, $h_z^- = -(1.8 \pm 1.5) \%$ for JLA.

This small forward-backward asymmetry is no more than a 1.6σ statistical effect and does not allow us to draw any relevant conclusion.

8 Outlook

8.1 Comparison with other observations

The Bianchi I metric is also used to decipher anisotropy in CMB data (Cea 2014) and in apparent proper motion measurements of extragalactic sources (Darling 2014).

Cea (2014) uses the axially symmetric Bianchi I metric to fit the Planck and WMAP data and finds an eccentricity at redshift $z = 1090$ of $e = (0.86 \pm 0.14) \cdot 10^{-2}$ and an eigendirection with galactic latitude of $\pm 17^\circ$. In our notations we have,

$$\beta = \sqrt{1 - e^2} - 1, \quad \eta = 0. \quad (129)$$

We use the first of equations (106) to compute β'_0 and the second of equations (124) to get the main Hubble stretch. Table 3 compares Cea’s results to ours. Although Cea’s Hubble stretch has the opposite sign and is smaller than ours by 8 orders of magnitude, the results are still compatible with each other.

Sample	CMB	Union 2	JLA
galactic longitude ($^\circ$)		88 ± 45	106 ± 16
galactic latitude ($^\circ$)	± 17	22 ± 26	1 ± 10
Hubble stretch in %	$(5.7 \pm 1.8) \cdot 10^{-8}$	-1.1 ± 1.1	-1.7 ± 1.3

Table 3: Cea’s fit (Cea 2014) (1σ errors) of Bianchi I with axial symmetry to CMB data compared with the two present fits.

Darling (2014) uses a tri-axial Bianchi I metric to fit the apparent motion, ‘drift’ for shortness, of 429 extragalactic radio sources measured by Titov & Lambert (2013) using Very Long Baseline Interferometry. Table 4 compares Darling’s results to ours. His main Hubble stretch has the same sign as ours but is ten time larger. Although the results are again compatible statistically, their head-on comparison raises a conceptual difficulty. Unlike

the Hubble diagram, drift measurements do depend on the peculiar velocity (and acceleration) of the observer and the separation of anisotropy induced by this peculiar velocity from anisotropic expansion at cosmological scale is delicate (Fontanini 2009). This is also true for measuring redshift distributions of quasars (Singal 2014).

Sample	drift		
ascension($^{\circ}$)	102 ± 24	13 ± 15	11 ± 33
declination($^{\circ}$)	1 ± 14	-47 ± 26	43 ± 26
stretch(%)	-19 ± 7	17 ± 7	2 ± 7
Sample	Union 2		
ascension($^{\circ}$)	126 ± 52	322 ± 67	48 ± 59
declination($^{\circ}$)	-58 ± 21	-33 ± 21	8 ± 32
stretch(%)	-1.5 ± 1.3	1.2 ± 1.1	0.3 ± 0.7
Sample	JLA		
ascension($^{\circ}$)	177 ± 56	34 ± 64	160 ± 30
declination($^{\circ}$)	-65 ± 14	-20 ± 20	28 ± 14
stretch(%)	-1.8 ± 1.4	1.1 ± 1.1	0.7 ± 1.0

Table 4: Darling’s fit (Darling 2014) (1σ errors) of tri-axial Bianchi I to the apparent proper motion (drift) of 429 extragalactic radio sources compared with the two present fits. For ease of comparison we have changed the sign of the second eigendirection in Union 2.

8.2 Future prospects

It is fair to say that all three observations, CMB, drift and Hubble diagram, pick up an intriguing signal of anisotropy when analysed in terms of a Bianchi I cosmology. All three signals fail to be significant. All three signals have some tension with each other. However two signals can look forward to exciting new data in the near future.

After a successful launch in December 2013, the satellite Gaia has started its five-year period of data taking. These data should reduce the error bars on the Hubble stretch measured through the drift of quasars from the present seven percent to one percent (Darling 2014).

We count on the Large Synoptic Survey Telescope (LSST) (Abell et al. 2009) to reduce the error bars in the Hubble diagram. LSST is a 6.7 meter telescope being built in Chile and that should start taking data in seven years. It will carry out a survey of 20 000 square degrees of the sky, essentially the southern hemisphere, in six photometric bands with a main cadence for observation of 3 to 4 days allowing discovery and sampling of light curve supernovae up to a redshift of about 0.8. The total number of SNe Ia in the main survey with a photometry sufficient for light curve fitting and photometric redshift measurement is of the order of 50 000 per year.

Let us see to what extent LSST can improve the present analysis. To this end, we simulate randomly 50 000 supernovae in 20 000 square degrees with a redshift distribution centered

around $z \approx 0.45$ and going up to $z \approx 0.8$. The magnitude error including intrinsic dispersion and photometric light curve fitting error is taken to be 0.12. The redshift error is set to $\sigma_z = 0.01(1+z)$ and is propagated to magnitude error.

Table 5 shows expected errors for 1 year and 10 years of LSST modelled by the tri-axial Bianchi I metric. Fiducial values for the main Hubble stretch parameter are taken to be 5σ away from zero for 1 year of LSST survey, and 3σ respectively 1σ in the two other principle directions. The main result is that after 10 years of LSST survey, stretch parameters can be estimated with an accuracy of about $3 \cdot 10^{-4}$ and the main eigendirection with an accuracy of a few degrees for a stretch parameter of the order of $3 \cdot 10^{-3}$.

Figure 3 shows the confidence level contours for axial and tri-axial Bianchi I metric fits with arbitrary color codes around the eigendirections on the celestial sphere for 1 year of LSST. All features observed in these figures are similar to those observed on real data. Bold black contours mark 68% confidence level and show the same kind of degeneracy as in figures 2. This is due to the very close values of the Hubble stretch parameters in the secondary eigendirections (\vec{u}_x, \vec{u}_y).

Sample	LSST 1 year				LSST 10 years			
	Axial	Tri-axial			Axial	Tri-axial		
Direction	\vec{u}_z	\vec{u}_x	\vec{u}_y	\vec{u}_z	\vec{u}_z	\vec{u}_x	\vec{u}_y	\vec{u}_z
ascension($^\circ$)	± 12	± 67	± 37	± 20	± 4	± 20	± 12	± 6
declination($^\circ$)	± 7	± 21	8 ± 8	± 9	± 2	± 7	± 3	± 3
stretch(%)	± 0.06	± 0.1	± 0.1	± 0.09	± 0.02	± 0.03	± 0.03	± 0.03

Table 5: 1σ errors for the two fits using axial and tri-axial Bianchi I metrics for 1 and 10 years LSST simulations with a tri-axial supernova distribution.

9 Conclusions

Today the Hubble diagram remains one of the cleanest windows on the Universe and still holds a lot of potential, both for data and theory. Indeed the underlying theory is simply general relativity together with a possibly weakened cosmological principle and allows for precise calculations. In view of the expected LSST data the Hubble diagram seems particularly well suited to separate geography from geometry in the sense of the Introduction.

References

- Abell P. A. et al., 2009, arXiv:0912.0201 [astro-ph.IM]
Amanullah R., Lidman C., Rubin D., Aldering G., Astier P., Barbary K., Burns M. S.,
Conley A. et al., 2010, ApJ, 716, 712
Amsler C. et al., 2008, Phys. Lett. B, 667
Antoniu I., Perivolaropoulos L., 2010, JCAP, 1012, 12

Betoule M. et al., 2014, arXiv:1401.4064 [astro-ph.CO]
 Campanelli L., Cea P., Fogli G. L., Marrone A., 2011, Phys. Rev. D, 83, 103503
 Campanelli L., Cea P., Fogli G. L., Tedesco L., 2011, Mod. Phys. Lett. A, 26, 1169
 Cea P., 2014, arXiv:1401.5627 [astro-ph.CO]
 Chang Z., Li X., Lin H.-N., Wang S., 2014a, Eur. Phys. J. C, 74, 2821
 Chang Z., Li X., Lin H.-N., Wang S., 2014b, Mod. Phys. Lett. A, 29, 1450067
 Darling J., 2014, arXiv:1404.3735 [astro-ph.CO]
 Fontanini M., West E. J., Trodden M., 2009, Phys. Rev. D, 80, 123515
 Jimenez J. B., Salzano V., Lazkoz R., 2014, arXiv:1402.1760 [astro-ph.CO]
 Kalus B., Schwarz D. J., Seikel M., Wiegand A., 2013, A&A, 553, A56
 Koivisto T., Mota D. F., 2008a, ApJ, 679, 1
 Koivisto T., Mota D. F., 2008b, JCAP, 0806,018
 Kolatt T. S., Lahav O., 2001, MNRAS, 323, 859
 Lewis A., Bridle S., 2002, Phys. Rev. D, 66, 103511, <http://cosmologist.info/cosmomc/>
 Mészáros A., Řípa J., 2013, arXiv:1306.4736 [astro-ph.CO]
 Quercellini C., Quartin M., Amendola L., 2009, Phys. Rev. Lett., 102, 151302
 Saunders P. T., 1969, MNRAS, 142, 213
 Schwarz D. J., Weinhorst B., 2007, A&A, 474, 717
 Singal A, K., 2014, arXiv:1405.4796 [astro-ph.CO]
 Titov O., Lambert S., 2013, A&A, 559, A95
 Tsaregorodtsev A. et al., 2008, J. Phys.: Conf. Ser., 119, 062048, <http://diracgrid.org>
 Yang X., Wang F. Y., Chu Z., 2013, arXiv:1310.5211 [astro-ph.CO]
 Enabling Grids for E-scienceE, <http://www.egi.eu>
 The MINUIT-ROOT analysis package, <http://root.cern.ch/drupal/>
 SIMBAD astronomical database: <http://simbad.u-strasbg.fr/simbad/>

Appendix: Elliptic integral

Consider the integral

$$I(z) = \int_0^z \frac{d\tilde{z}}{\sqrt{g(1+\tilde{z})^3+1}} \quad z \geq 0. \quad (130)$$

Its computation follows from Mészáros & Řípa (2013). The change of variables,

$$v = \frac{1}{1+\tilde{z}}, \quad (131)$$

gives

$$I(z) = \int_{(1+z)^{-1}}^1 \frac{dv}{\sqrt{v}\sqrt{g+v^3}}, \quad (132)$$

followed by

$$v = g^{1/3} y, \quad I(z) = g^{-1/3} \int_{g^{-1/3}(1+z)^{-1}}^{g^{-1/3}} \frac{dy}{\sqrt{y}\sqrt{1+y^3}}. \quad (133)$$

Following Mészáros & Řípa (2013) let us define

$$\cos(\theta(z)) := \frac{1+z - (\sqrt{3}-1)g^{-1/3}}{1+z + (\sqrt{3}+1)g^{-1/3}}, \quad (134)$$

which finally yields

$$I(z) = 3^{-1/4} g^{-1/3} \left(F(\theta(0), k) - F(\theta(z), k) \right), \quad k^2 := \frac{2+\sqrt{3}}{4} < 1. \quad (135)$$

The elliptic integral (of first kind) is defined by

$$F(\phi, k) := \int_0^\phi \frac{du}{\sqrt{1-k^2 \sin^2 u}}. \quad 0 < k^2 < 1. \quad (136)$$

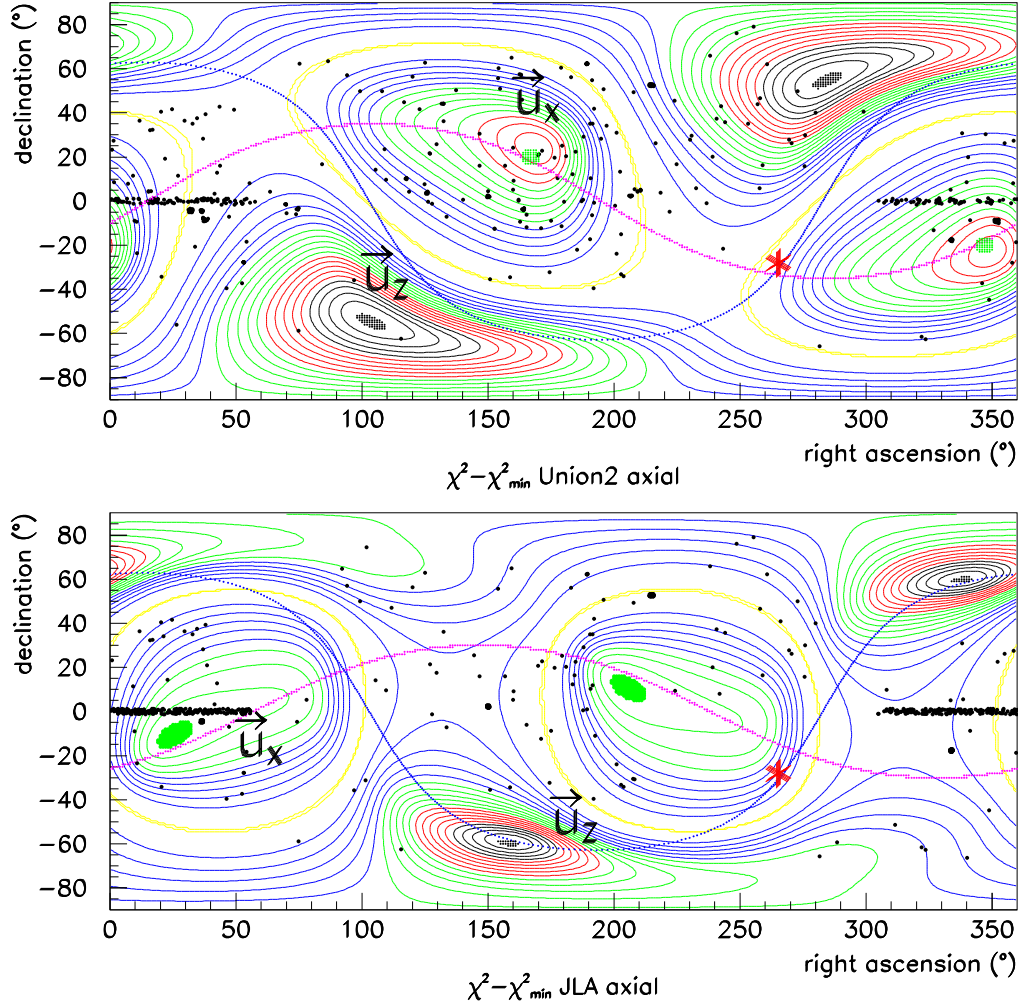


Figure 1: Confidence level contours of privileged directions in arbitrary color codes for Bianchi I spacetimes with axial symmetry. Black points represent supernova positions. Note the accumulation of supernovae in the equatorial plane. The blue line is the galactic plane and the purple line is the plane transverse to the main privileged direction \vec{u}_z (gray speck). The green specks show the secondary directions. The red star is the direction towards our galactic center.

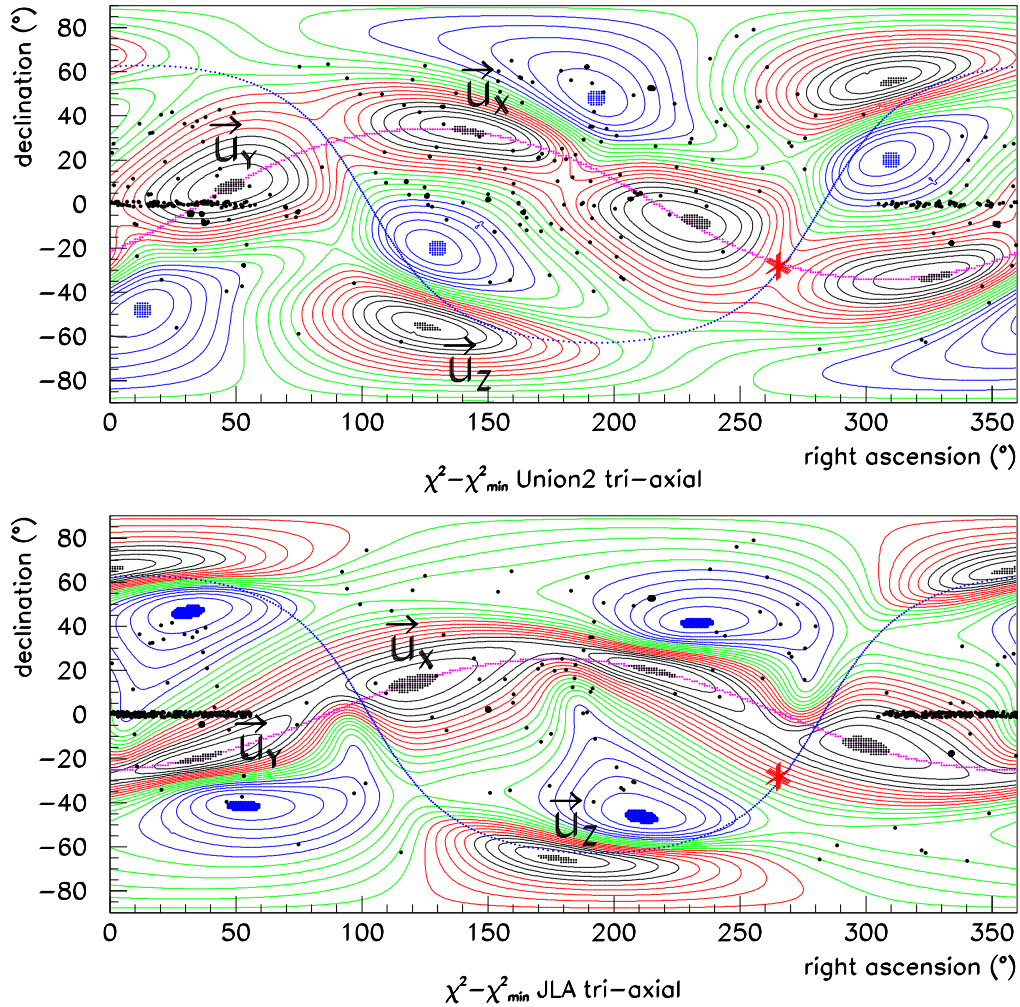


Figure 2: Confidence level contours of privileged directions in arbitrary color codes for the tri-axial Bianchi I metric. Black points represent supernova positions. Note the accumulation of supernovae in the equatorial plane. The blue line is the galactic plane and the purple line is the plane transverse to the main privileged direction \vec{u}_z (gray speck). Blue specks correspond to regions where χ^2 is maximum. The red star is the direction towards our galactic center.

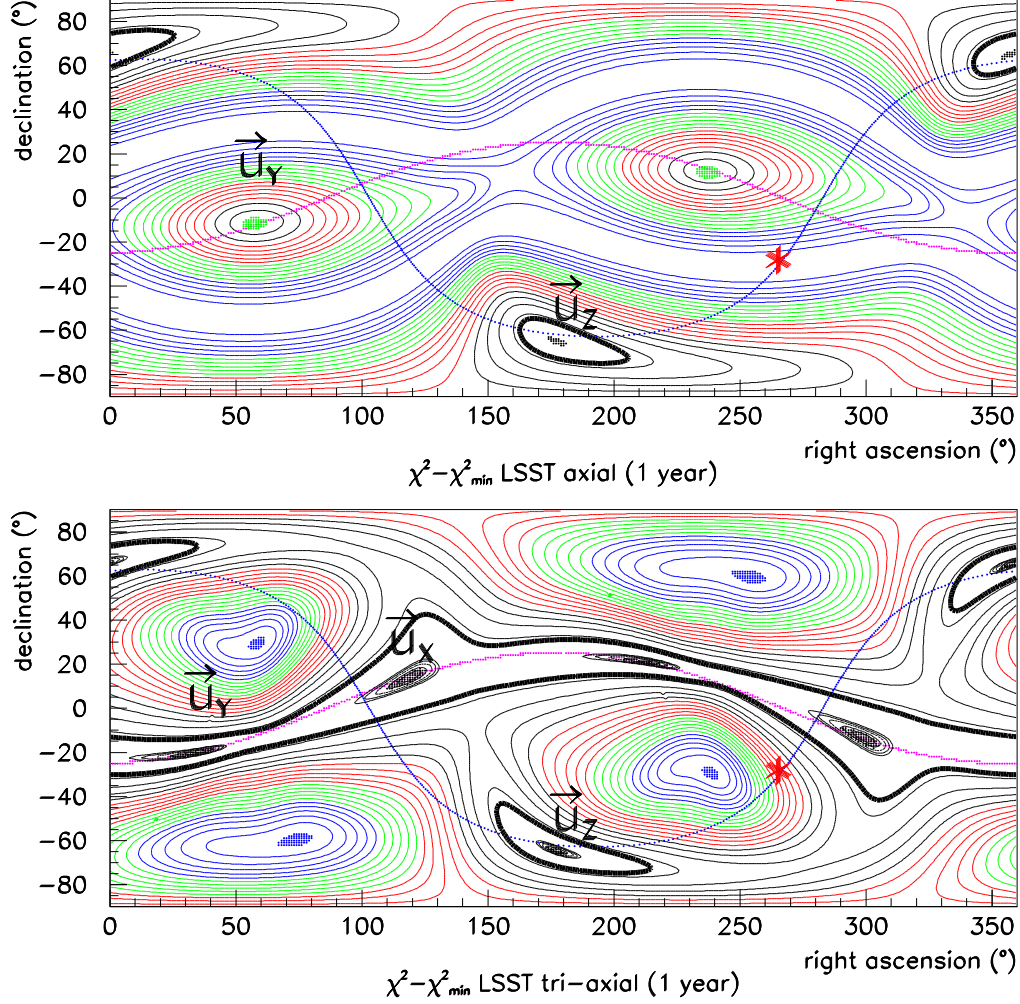


Figure 3: Confidence level contours of privileged directions in arbitrary color codes for the two fits using the axial and tri-axial Bianchi I metric for one year of LSST. 68% confidence level contours are drawn in bold. The blue line is the galactic plane and the purple line is the plane transverse to the main privileged direction \vec{u}_z (gray speck). The red star is the direction towards our galactic center. The green specks in the upper plot show the secondary directions in the axial fit while the blue specks in the lower plot show regions where χ^2 is maximum.